

Electrochemical Impedance Spectroscopy Studies on Hydrogen Evolution from Porous Raney Cobalt in Alkaline Solution

Dario Delgado¹, Manickam Minakshi^{1*}, Dong-Jin Kim²

¹ School of Engineering and Information Technology, Murdoch University, Murdoch, Australia

² Mineral Resources Research Division, Korea Institute of Geoscience and Mineral Resources, Daejeon, South Korea

*E-mail: minakshi@murdoch.edu.au

Received: 29 July 2015 / Accepted: 28 August 2015 / Published: 30 September 2015

The hydrogen economy has gained increasing attention from government bodies and major oil companies. There are proven examples of this technology being implemented in a society like Iceland, where electrolytic hydrogen generation powered by renewable energy has been developed to support the demand of the transportation sector. Hydrogen generation via electrolysis consists of the hydrogen and oxygen evolution reactions. Conventional electrode materials used for the electrolysis belong to the platinum group metals that are expensive. In this work, Raney cobalt as an alternative which is inexpensive, electrodeposited from a Watts bath is reported. In addition, modifying the Watts bath composition and combining two types of Raney have also been investigated and reported. We have identified overpotentials of -349 mV for the best Raney cobalt sample and -270 mV when Raney nickel is combined with Raney cobalt for hydrogen evolution in alkaline medium at 100 mA cm⁻². Another objective of this work is resolving the difficulties found in interpreting the electrochemical impedance data for Raney type materials. The nickel binder competes with Raney cobalt during the reaction, these interactions exhibit different impedances. The electrodeposited electrodes have been tested for energy efficiency with overpotential curves and electrochemical impedance measurements. Additional tests including X-ray diffraction and field emission scanning electron microscopy equipped with energy dispersive analysis have also been undertaken that support the results of the catalyst surfaces under study.

Keywords: modified Watts Bath, Raney cobalt, hydrogen evolution.

1. INTRODUCTION

Recently, hydrogen has received increased attention from major oil companies like Exxon Mobil [1], Shell [2, 3] and BP [4]. Hydrogen is a source of energy to support society. These oil companies, in their energy outlook reports, point out a more diversified future for energy supply mix in

which hydrogen participates to a large extent. The energy outlooks for 2030 made by Exxon Mobil and BP indicate emerging alternative sources of energy; for example BP comments that ‘the fastest growing fuels are renewables (including biofuels)’. The Shell energy outlook speculates hydrogen fuel cell vehicles (FCVs) will compete with electric vehicles in 2050, implying that the hydrogen technology could dominate the market of transportation. Iceland, which has important sources of geothermal energy, generates hydrogen electrolytically, this process being powered by renewable energy. The Shell Company has supported the development of this technology in Iceland. Most of its generated hydrogen supplies the demand of the transportation sector. This is an important example that asserts successful application of this technology in a society.

Electrolytic hydrogen generation is energy intensive and expensive. Conventional materials for water electrolysis belong to the platinum group metals that are expensive. In this respect, our current work focuses on developing alternative electrode materials to substitute those of which are conventionally used now. Cobalt and nickel are alternative materials as they are less expensive and electrochemically active toward the hydrogen evolution reaction (HER) [5]. There are two approaches in improving the electrochemical activity of materials, these are known as the ‘geometric’ and ‘electronic’ factors [6]. Cobalt and nickel in the form of powder alloys with aluminum or zinc are called Raney after activation. Raney cobalt or nickel, has a high geometric factor as its surface area per unit of mass is substantially higher than the pure material itself. Raney cobalt and nickel were initially developed for organic reactions as catalysts [7-10]. The synthesis of Raney Co and Ni for electrode applications differs from that used for organic reactions [7-12]. The most common synthesis for Raney Co and Ni is by electrodeposition, where the powder alloy is deposited on the surface of an electrode along with Ni from the plating bath (i.e. acting as the binder), then it is activated.

Watts bath is the most common plating solution used for the purpose of depositing powder alloys [13]. In our current work, we have employed and reported a “*modified version*” of the Watts bath [14]. The Raney Co electrodes electrodeposited by the modified Watts bath are evaluated to determine their energy efficiency (refer to “*Joule’s effect*”) toward the HER in alkaline medium. In addition, the electrochemical impedance spectroscopic (EIS) technique gives useful information about how the energy is being consumed (i.e. size of the electric resistance) and EIS data is interpreted with linear voltammetry. The challenging issue is EIS data fitting, particularly when the binder competes with the catalyst (i.e. Raney cobalt or nickel). The electrochemical impedance analysis and the improved overpotential for the electrodeposited Raney Co and Raney Co/Ni mix are reported here. Further to this, the influence of the catalyst surface roughness and its effect in energy efficiency is also detailed in this work.

It is reported by Hitz [15] that Raney Ni/Al and Ni/Zn electrodes exhibited overpotentials ranging from -268 to -521 mV at a current density 100 mA cm^{-2} at 25 °C in 1 M NaOH. In the case of a nickel plate an increase in overpotential to -530 mV is reported [16]. Further improvement in the overpotential has also been reported [13, 17] well below -100 mV, however, this has been achieved only at a higher temperature of 90 °C. It is generally accepted that a decrease in $\sim 20 \text{ mV}$ of overpotential is reasonable, for every 10 °C of increase in temperature in the alkaline solution. The overpotentials identified from our work on Raney Co which presented here are competitive to those published earlier [5] for this specific type of material.

To the best of our knowledge, no work has been reported on the use of Raney Cobalt in modified Watts bath for the hydrogen evolution reaction. A brief theory of the hydrogen evolution reaction, which commonly takes place in alkaline media during electrolysis, is given in the next section for the benefit of readers rather than solely referring to the literature.

2. THEORY

Electrolytic hydrogen evolution in alkaline media has three well-known mechanism steps, described by Eqs. 1-3 and its corresponding HER schematic diagram is shown in Fig. 1 (Tafel step not shown).

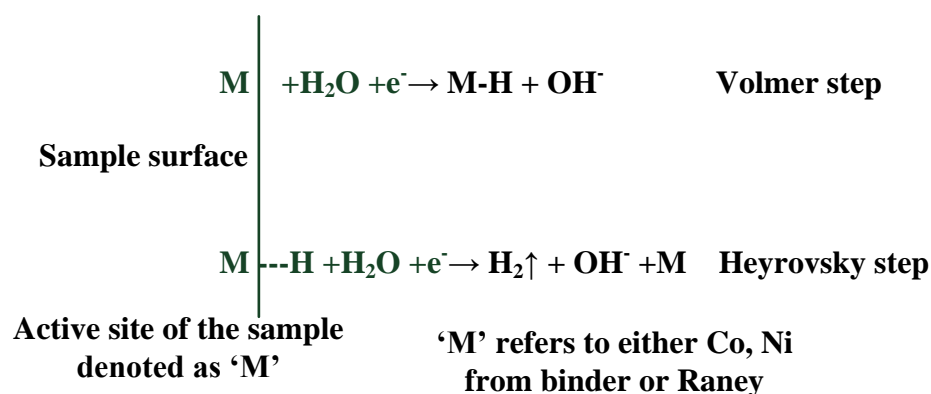


Figure 1. HER Schematic diagram on the Catalyst surface

In these Equations, 'M' denotes the active site on the catalyst, and they show atomic hydrogen as the only reaction intermediate. Hydrogen can only evolve in Eqs. 2 and 3, either as a combination or through one of these two steps. When a particular step is rate determining (rds), discrete Tafel slope values (*b*) are found. A Tafel slope of 120, 40 and 30 mV dec⁻¹ represents Eqs. 1, 2 and 3 as the rds, respectively. To reconcile other slope values, modifications to the mechanism or the introduction of different isotherms are required [6, 18-20].

In addition to a Tafel slope analysis, electrochemical impedance spectroscopy shows characteristics of the hydrogen evolution reaction (HER). EIS technique give us a wide range of information, for example, there has been relevant studies about the pore shape by EIS [15, 21]. Tafel slopes has been reconciled in terms of pore shape in some cases [22]. EIS equivalent circuit models for

hydrogen evolution on Raney type surfaces have been mathematically explained in detail by Lasia [22-24]. The most common models used for the HER on porous surfaces such as Raney Co in alkaline medium, are shown in Fig. 2 [15, 23, 25-30].

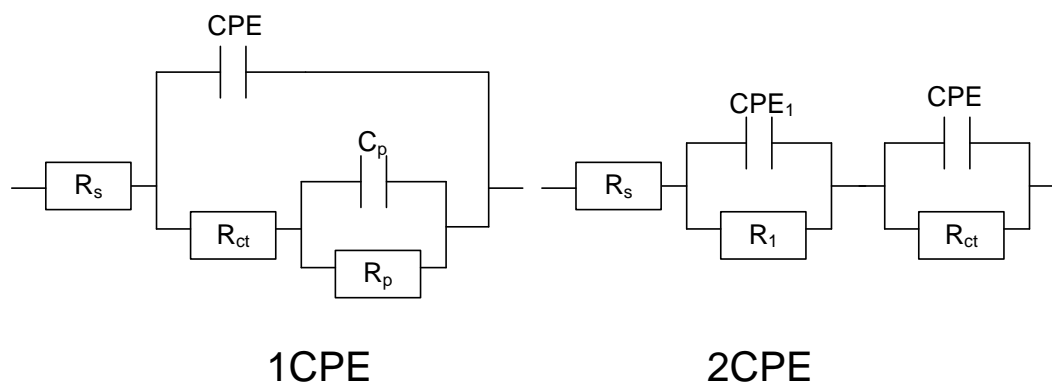


Figure 2. Equivalent circuit models for the HER on porous surfaces.

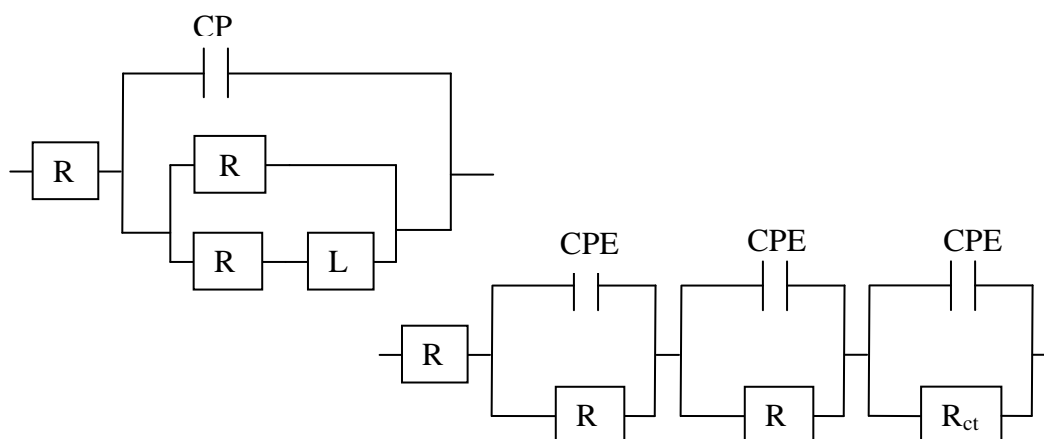


Figure 3. 3CPE equivalent circuit used for the HER in the presence of an inductive loop [24], and modified 2CPE to account for the impedance of an oxide layer.

The 2CPE model is the preferred one for data fitting by Lasia [15]. The reason for the 2CPE model being preferred for EIS fitting of porous surfaces, lies on the physical meaning of CPE_1 and R_1 . They represent characteristics of the surface geometry of the porous electrode, although its specific meaning is not always clear [15]. The 1CPE model has been used for the case of Raney Co [27], however, it is less frequently used for EIS data fitting of porous surfaces. It should be noted that the 1CPE and 2CPE models are equivalent.

There is a third model that we have called 3CPE which is shown in Fig. 3. This model also has mathematical support and it can occur for reactions of one adsorbed specie [24]. A circuit is inductive when its phase (Z) is positive, this means that the voltage leads the current. This is the reason why the 3CPE model has an inductor (L). One example of inductive impedance is shown in the next section

(Sec. 4, Results and Discussion), Fig. 5 (top left), where it is shown that at low frequencies, the phase (Y) is negative, this means a positive phase (Z). A distinction should be made between the 1CPE and 3CPE models. The main difference between these two models is related to the magnitude of the equilibrium constants of the Eqs. 1-3. When the magnitude of the forward and reverse equilibrium constants of the first step (e.g. Volmer as rds) are bigger than those from the second step (e.g. Heyrovsky), one would expect the absence of inductive behavior on impedance plots. Vice versa, for instance, if Heyrovsky is the rds then a decrease in the Tafel slope should accompany the presence of an inductive loop.

The electrical elements of these equivalent circuits have a discrete meaning. In all models, CPE is a constant phase element related to the double layer capacitance (C_{dl}) and R_{ct} is the charge transfer resistance. CPE and R_{ct} are related to chemical processes on the surface of the electrode. C_p and R_p are closely dependent on the kinetics of the HER reaction, specifically to the values of the rate constants of Eqs. 1- 3. The CPE_1-R_1 combination is related to the porosity of the electrode and found to be independent of the kinetics of the faradaic process [30]. The CPE_f-R_f combination represents the impedance of an oxide layer. Finally, R_s is the solution resistance.

The double layer capacitance is used to determine the degree of porosity of the Raney materials. In this respect, it has been taken an estimated C_{dl} of $20 \mu F cm^{-2}$ for a smooth metallic electrode to determine a ratio between this theoretical value and the experimentally determined C_{dl} for porous electrodes to obtain a roughness factor r_f [28]. The obtained roughness factor (r_f), illustrating the porosity, for these materials are tabulated in Table 3. The below Eq. 4 determines the average double layer capacitance of porous surfaces for one adsorbed specie reactions.

$$T = \bar{C}_{dl}^{\phi} (R_s^{-1} + R_{ct}^{-1})^{1-\phi} \quad (1)$$

The parameter T is related to the double layer capacitance and ($T = C_{dl}$ when $\phi = 1$) [15]. The variable ϕ is associated to an angle of depression ($1-\phi$) of the capacitive loop to account for non-idealities. Deviations from the ideal capacitance are expected as the substrate is heterogeneous; there could be lateral effects or partial transfer of charge between adsorbed molecules and the substrate [6]. Common values of ϕ are found ranging from 0.75 to 0.97 on porous surfaces for the HER [15].

3. MATERIALS AND METHODS

3.1. Electrode preparation

The plating station consists of copper and nickel plates, acting as working and counter electrodes, respectively, a power supply, hot plate with magnetic stirrer and the plating solution. One face of the copper electrode is insulated with ferro-laquer, before electrodeposition, it is cleaned with the following procedure. It is polished with fine emery paper, degreased with acetone, alkaline electrocleaned with 1.5 M NaOH solution for 1 minute at $30 mA cm^{-2}$ at ambient temperature. Then it is acid pickled with HCl 10% for 5 seconds. After cleaning, the copper panel is plated with nickel

binder at a current density of $i = 30 \text{ mA cm}^{-2}$ for 20 minutes, and the composition of the Watts bath is shown in Tables 1 and 2. Raney cobalt precursor was acquired from Sigma-Aldrich in the form of cobalt-aluminum alloy powder, with a Co to Al ratio as 79:21 by mass. The Raney nickel particles were acquired from Merck having a composition by mass of Ni-Al 50:50. Cobalt and nickel particles are 150 micron max in size. As a safety measure, both Raney types were acquired inactive as they are pyrophoric. After deposition the coating was activated in 6.25 M NaOH solution at 70 °C for 1h.

Table 1. Plating characteristics of the Raney Co electrode

Solution ID	Temperature (°C)	Time (min)	Reagents (Analytical grade)	Concentration g l ⁻¹
Watts Ni	55	20	NiSO ₄ ·6H ₂ O	300
			NiCl ₂ ·6H ₂ O	45
			H ₃ BO ₃	30
Watts Ni 1/2/3	55	20	NiSO ₄ ·6H ₂ O	350
			NaCl	148/100/40
			H ₃ BO ₃	30

All solutions were vigorously stirred by a magnetic stirrer.

Table 2. Description of the cobalt and nickel particles coating application

Sample ID	Preparation	
	Raney Co or Ni concentration (g l ⁻¹)	Solution ID
Ni plate	Acquired	
Raney Co 1	6.25	Watts Ni
Raney Co 2	12.5	
Raney Co 3	25.0	
Raney Co 4		Watts Ni 3
Raney Co 5	25.0	Watts Ni 2
Raney Co 6		Watts Ni 1
Raney Co/Ni 7	6.25*	Watts Ni
Raney Co/Ni 8	12.5*	
Raney Co/Ni 9	25.0*	

*Raney Co to Raney Ni added into the Watts bath in a ratio of 50:50 by mass.

3.2. Linear Voltammetry

A three electrode set up consisting of the Raney Co or Co/Ni electrode (10 x 20 x 1 mm), platinized platinum plate (50 x 50 x 1 mm) and Argental sat'd KCl as the working, counter and reference electrodes, respectively. These electrodes were coupled to a BioLogic VSP potentiostat to register the data. The reference electrode was placed in the vicinity of the working electrode (~2 mm) with a Luggin capillary and the IR_{drop} compensation was done by the current interruption method. The

alkaline medium was 2 M KOH at 25 °C. The current density range was set from 1 to 100 mA cm⁻² and the scan rate was 0.1 mV s⁻¹.

3.3. Electrochemical impedance spectroscopy

This test was done in sequence after linear voltammetry under the same set up. EIS is done with a stabilization time between working potentials of 3 min, potential amplitude of 5 mV and a frequency range of 20 kHz to 0.05 Hz. A fit for purpose Argental sat'd KCl reference electrode (RE) was used (a typical assembly of the RE is shown in [31]).

3.4. Surface tests

The morphology of the deposits was examined by field emission scanning electron microscopy (FE-SEM) equipped with energy dispersive analysis (EDS) for qualitative elemental analysis using a JEOL JSM-7000F FE-SEM/EDS instrument. The crystal structure and chemical composition of the deposits were analyzed by a Siemens X-ray diffractometer (XRD) with Philips Co-K α radiation (1.7902 Å).

4. RESULTS AND DISCUSSION

4.1. Tafel plots

The electrochemical and kinetic parameters of the samples examined in 2 M KOH for hydrogen evolution is given in Figure 4 and Table 3.

Table 3. Experimental kinetic parameters of the samples for the HER in 2 M KOH (per apparent area)

Raney Co or Co/Ni sample ID	$-b$ (mV dec ⁻¹)		$- \eta_{100}$ (mV)	R_{ct}^* at η_{10} (Ω cm ²)	r_f^* at η_{10}
	low η	high η			
1	98	171	378	--	--
2	100	128	349	--	--
3	98	98	352	--	--
4	112	146	359	--	--
5	101	160	386	--	--
6	112	143	354	--	--
7	128	179	313	1.821	630
8	126	191	270	1.539	1648
9	117	162	271	3.695	412

*: Rounded up values based on their standard deviations.

Three samples of Raney Co and three samples of Raney Co/Ni have been compared in Fig. 4, along with the nickel plate. Among the six Raney Co samples that have been electrodeposited (see

Tables 1-3 for details), only three (Co 4, 5 and 6) are shown in Fig. 4 and the rest (Co 1, 2 and 3) are shown only in Table 3. Samples labeled (a) to (c) contain only cobalt particles and nickel binder. Relatively high overpotentials have been observed for the samples (a) to (c) and this has made difficult to fit impedance data, as the nickel binder (from Watts bath; see Table 1 for details) competes with the Raney Co particles for the HER. For this reason, fitted impedance parameters have not been processed for samples a–c.

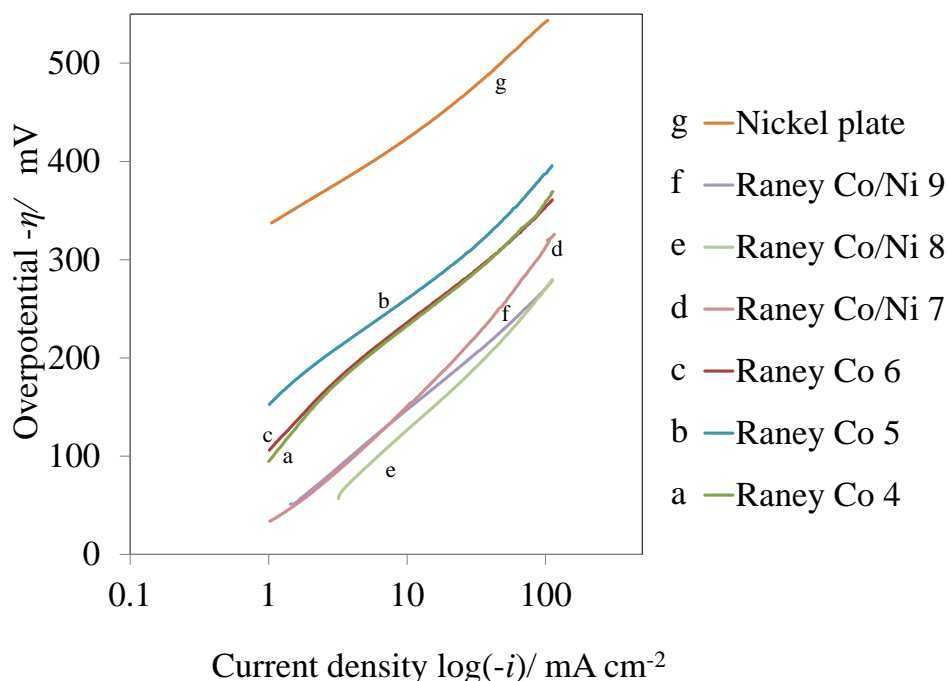


Figure 4. Experimental HER Tafel plot for selected samples in 2 M KOH at a sweep rate of 0.1 mV s^{-1} .

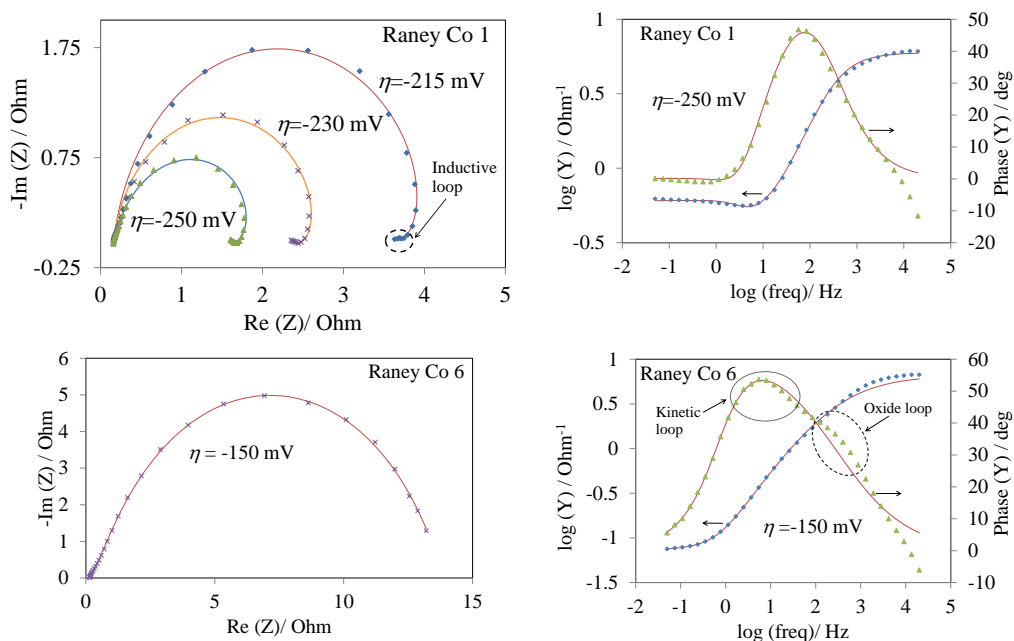


Figure 5. Nyquist and Bode admittance diagrams of the samples 1 and 6 for the HER in 2 M KOH solution. Continuous lines represent the fitted curve by the 3CPE model for the sample 1 and modified 2CPE model for the sample 6, experimental data as symbols.

However, selected impedance spectra have been shown for these samples (in the next section 4.2) to illustrate differences between fitted curves and experimental points. The best samples in terms of overpotential are those which contain Raney Ni particles in the mix, these being samples (d) to (f). These mixed samples are substantially better than those with only Raney Co. This shows that Raney nickel is more active than Raney cobalt for the HER in alkaline solution. Considering Tafel slopes, samples containing only Co particles (i.e. samples a–c) show smaller slopes at low overpotentials than those with Ni particles. This could be explained as follows.

A slope of 120 mV dec^{-1} can only be explained considering Volmer (i.e. Eq. 1) as the rds. Whereas, slopes of smaller magnitudes indicate Heyrovsky (i.e. Eq. 2) competing with Volmer. This is supported by EIS where the Raney Co 1 sample shows an inductive loop in the Nyquist diagram as shown in Fig. 5. Inductive loops are an indication that Heyrovsky is competing with Volmer as the rds, this was described in the theory section where the 3CPE circuit was outlined.

The next variable of interest is the oxygen content. Oxygen content does not affect the overpotential for the HER on Raney Co coatings, and this is different from those results found for Raney Ni [31]. The reason for this result is the high R_{ct} values found for Raney Co, which is supported by its relatively high overpotentials for the HER. Hitz [15] reported R_{ct} values which are in agreement to those observed here in this work. Nickel binder with high oxygen content has shown electrical resistances (R_f) as large as $0.5 \Omega \text{ cm}^2$ [31]. This oxide resistance is significantly smaller than the R_{ct} value ($14.6 \Omega \text{ cm}^2$) shown for the Raney Co 6 sample at $\eta = -150 \text{ mV}$ shown in Fig. 5. Most of the overpotentials found in the samples 1 to 6 are dominantly controlled by their R_{ct} , this explains why, despite of samples containing high oxygen content, their overpotentials cannot be explained in terms of the additional impedance from the oxide loop.

4.2. Electrochemical impedance spectroscopy plots

Based on the facts explained in the previous section 4.1, we have focused our studies only on the samples (d – f in Fig. 4) for EIS data processing. This set of samples show lower overpotentials when compared to the other samples which contain only cobalt (a – c in Fig. 4). The nickel binder does not compete with the Raney Co/Ni mix catalyst which makes a better fitting for the EIS data. However, we show selected impedances for samples Co 1 and Co 6 to describe the conflicts found when performing EIS data fitting. Figures 5 to 8 show the Nyquist impedance and Bode admittance of selected Raney samples. Figure 5 compares the impedances of the Raney Co 1 and Co 6 samples. The impedance spectra for sample 1 show inductive loops, in addition to having a lower Tafel slope. The sample 1 was prepared with the smallest concentration of Co particles (i.e. 6.25 g l^{-1}) and it is the only sample which shows inductive loops. The formation of inductive loop suggests that the nickel as the binder is competing with Raney Co. Figure 5 also includes the impedance spectra of the sample Co 6, and it does not show any inductive behavior (absence of negative phase (Y)), while it shows an additional capacitive loop in a frequency region where oxides could manifest. This oxide loop appears as a shoulder in the Bode admittance diagram (in Fig. 5) at a log of the frequency between 2 and 3.

This sample shows the highest amount of oxide by EDS analysis which quantified as high as 7.83%, among all the Raney samples studied, tabulated in Table 5.

Table 4. 2CPE modeled data of the Raney Co/Ni 8 sample for alkaline HER with a solution resistance of $R_s = 0.2 \, \Omega$.

$-\eta$ (mV)	CPE_{dl} ($F \, s^{\phi-1} \, cm^{-2}$) $\ast 10^{-2}$	ϕ_{dl}	R_{ct}^* ($\Omega \, cm^2$)	CPE_1 ($F \, s^{\phi-1} \, cm^{-2}$) $\ast 10^{-2}$	ϕ_1	R_1^* ($\Omega \, cm^2$)
60	2.33		1.778	5.07	0.62	7.644
100	1.59	1	1.519	6.02	0.60	2.861
155	1.40		1.257	5.17	0.62	1.786

* additional significant figures due to smaller standard deviations.

Table 5. Oxygen elemental dispersive analysis of the Raney Co and Co/Ni electrodes

Concentration by mass (%)	Raney Co or Co/Ni sample ID									
	1	2	3	4	5	6	7	8	9	
Oxygen	1.70	5.23	3.98	0.89	2.16	7.83	2.14	2.34	1.13	

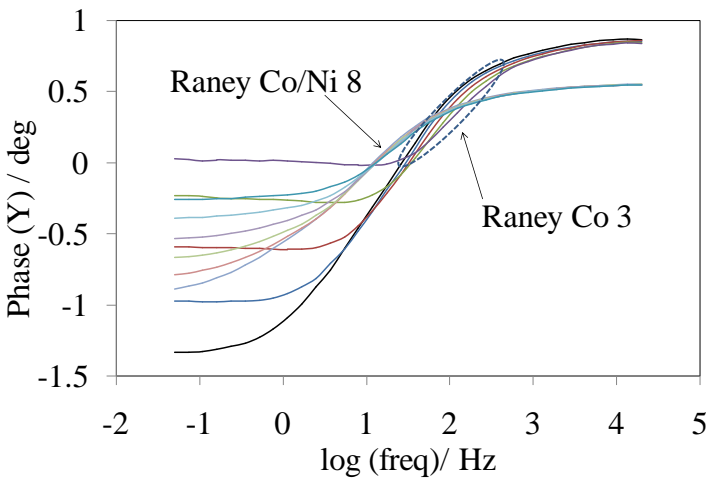
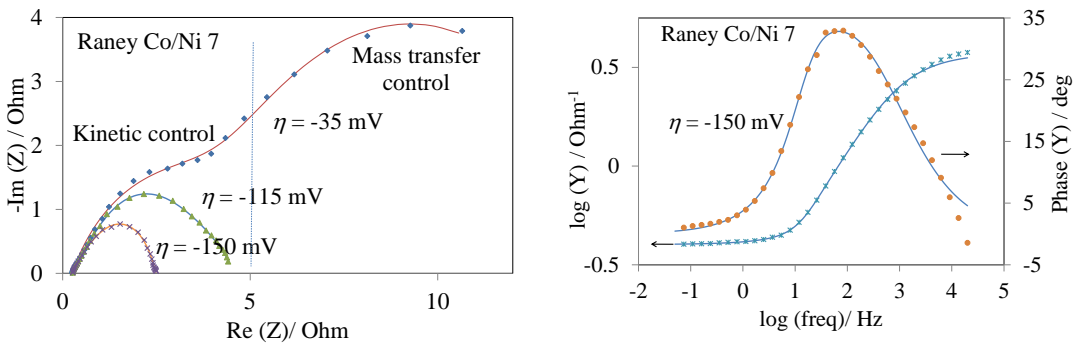


Figure 6. Experimental Bode admittance diagram of the samples 3 and 8 for the HER in 2 M KOH solution.



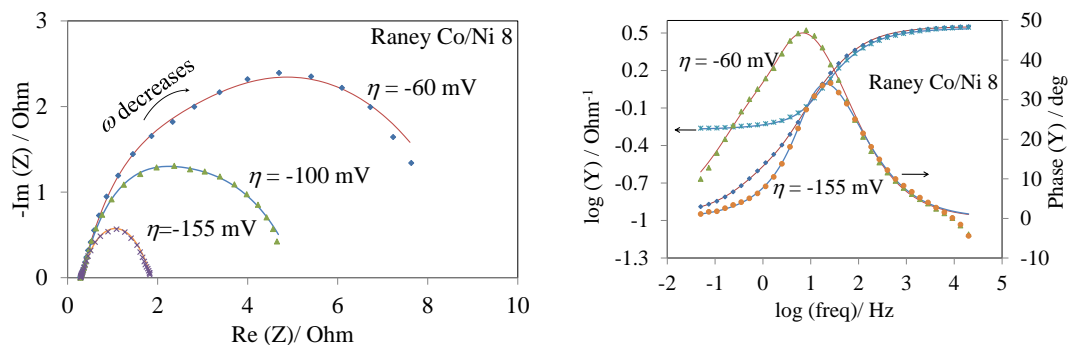


Figure 7. Nyquist and Bode admittance diagrams of the samples 7 and 8 for the HER in 2 M KOH solution. Continuous lines represent the fitted curve by the 2CPE model for both samples, experimental data as symbols.

The modified 2CPE model (i.e. an additional capacitive loop added to this model) failed to fit the experimental data of the sample 6 as most of the experimental points do not intersect the fitted curve. In Raney Co samples when the nickel binder competes for the HER, these samples do not yield a good EIS data fitting as the Ni binder and the Co catalyst have different impedances for the HER, and hence the 2CPE model may not be suitable.

The difficulty in fitting EIS data for the samples containing only Raney cobalt is that the nickel binder competes with the cobalt catalyst and this is again demonstrated in Fig. 6. The data in Figure 6 shows that at the frequency region where the charge transfer impedance manifests, no constant slope is observed for sample 3, whereas for sample 8 it shows a constant slope for all the cycles shown. This indicates that there is one dominant type of interaction between one of the Raney types (i.e. nickel or cobalt) and the HER for the sample 8. This is not the case for the sample 3, which is believed that the HER occurs on a combination of the nickel binder and Raney Cobalt as a function of overpotential. This combination of the HER occurs on different materials as a function of overpotential could explain why it is difficult to fit EIS data for the samples 1 to 6.

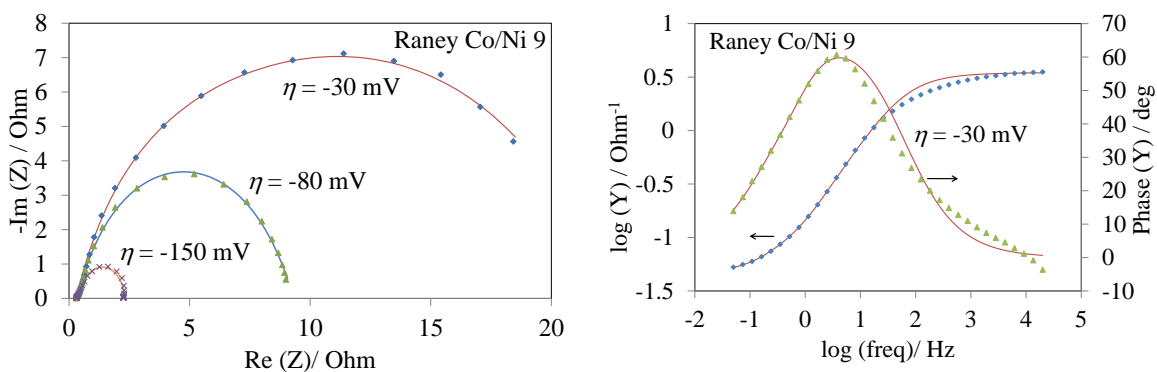


Figure 8. Nyquist and Bode admittance diagrams of the sample 9 for the HER in 2 M KOH solution. Continuous lines represent the fitted curve by the 2CPE model, experimental data as symbols.

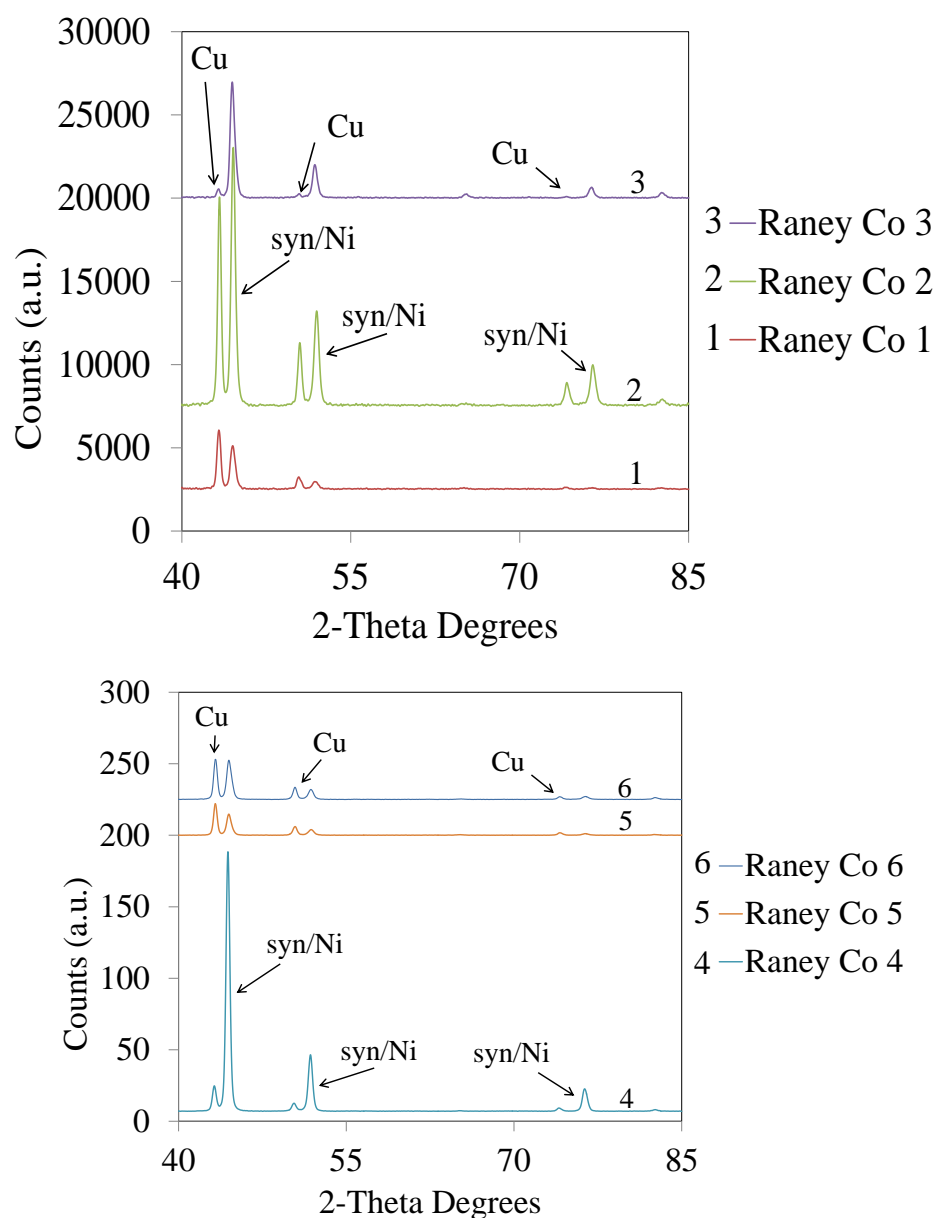


Figure 9. X-ray diffraction spectra of the Raney Co samples.

Samples containing Ni particles in the mix (i.e. Raney Co/Ni samples 7 to 9) show better EIS data in terms of model fitting. The parameters used for the curve fitting for sample 8 are shown in Table 4. The EIS fits improve at higher overpotentials where Ni particles become the dominant location for the HER. At low overpotential ($\eta = -35$ mV), for sample 7, two regions corresponding to kinetic and mass transfer have been indicated [32] in Fig. 7 while for high overpotential ($\eta = -150$ mV) the kinetic loop becomes dominant. Fig. 7 shows that the higher the overpotential, the better the fit for sample 8. However, the EIS data from samples 7 to 9 is difficult to fit at low overpotentials, one example is shown in Fig. 8 (i.e. Bode admittance at $\eta = -30$ mV). There is a region where a slight discrepancy is observed in the fit (i.e. missing a few of the experimental points). As discussed earlier, when two materials compete for the reaction then the model may not be appropriate. The CPE model series have been developed for one type of reaction intermediate, $M-H$ as shown in the mechanism

steps in Fig. 1. In the region of interest, being around η_{10} (cf. Fig. 4) the fits improve substantially as shown in Figs. 7–8. This supports the reasoning that Raney Ni is more active than Raney Co and the nickel binder.

4.3. X-ray diffraction (XRD) spectra

To identify the nature of oxygen species associated with the metal present in the Raney samples, XRD characterization has been carried out. The XRD spectra of the Raney Co and Co/Ni samples are shown in Figures 9 and 10 respectively. The important feature to note is the intensity observed for the patterns corresponding to Raney Co and Co/Ni samples studied. They differ substantially in their counts (see y-axis of the figures) for the samples labeled between 1 and 3; 4 and 9. Therefore they have been placed into separate figures for a peak resolution. Nevertheless, all the samples show the characteristic Ni peaks (from Ni binder in the case of samples between 1 and 6) and these have been indicated in the figures. The peaks corresponding to Cu comes from the copper substrate in addition to the synthetic nickel peaks.

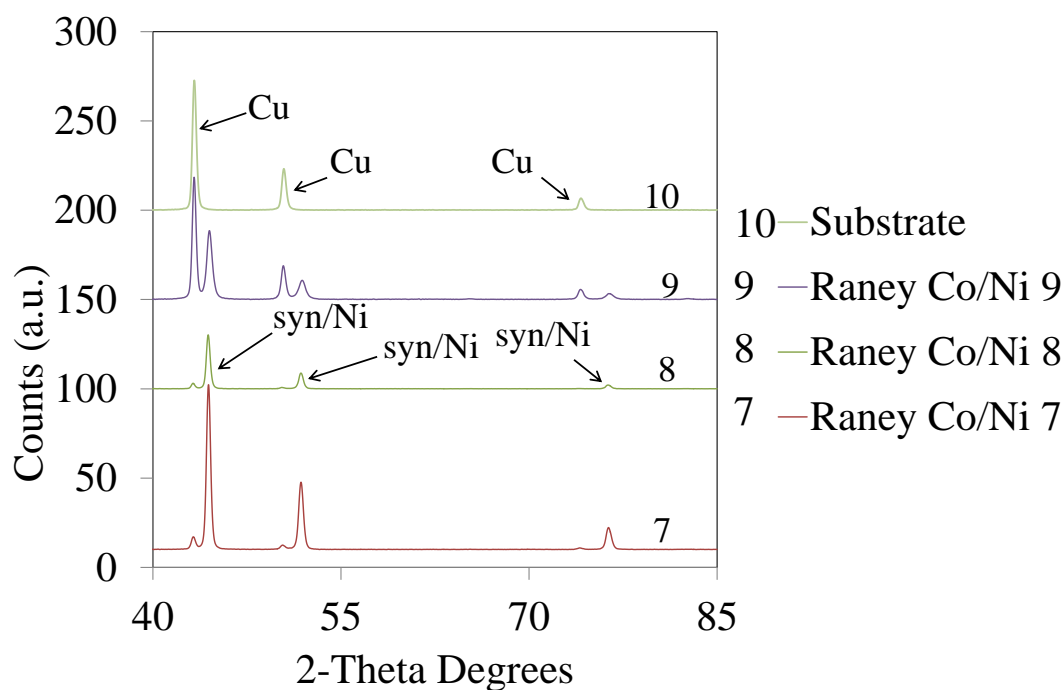


Figure 10. X-ray diffraction spectra of the Raney Co/Ni samples.

There is no evidence of other elemental peaks including metal oxide present in Raney samples through XRD diffraction pattern. Interestingly, peaks corresponding to cobalt were not identified by XRD; it should be noted that if the cobalt peaks are present, then these would have been overlapped with the Ni peaks, as they lie close to each other. After a careful analysis, no peaks relating NiO or CoO have been identified but EIS suggest that the presence of oxygen in the samples could be in the form of nickel oxide. Previous studies [31] has shown that XRD may not be a viable tool to identify

low concentration of oxides while XPS may aid the presence of oxygen O(1s) in the form of nickel oxide and hydroxide from Watts plating solutions. As XRD is not feasible, alternatively, we have used FE-SEM associated with EDS to analyze the oxygen content in the samples.

4.4. Field emission scanning electron microscope (FE-SEM) analysis

Figure 11 shows the porous micrograph of the Raney Co/Ni sample 8, which is the most energy efficient for the HER among all the samples investigated (*cf.* Table 3). The observed morphology is the common pattern seen for all the sample surfaces studied. The observed porous-type morphology supports the use of EIS fitting constructed for porous surfaces. Table 5 shows the elemental dispersive analysis (EDS) for oxygen content associated with FE-SEM. High concentrations of NaCl (from Watts bath) are detrimental for the deposition of the binder as it increases the oxygen content of the coating while increasing the electrical resistance. The modification in the Watts bath, by substituting $\text{NiCl}_2 \cdot 6\text{H}_2\text{O}$ for NaCl, is a satisfactory option as it decreases the oxygen content in the coating when the concentration of NaCl is in the range of 40 g l^{-1} . This is supported with results found from the sample 4 which shows the smallest percentage of oxygen.

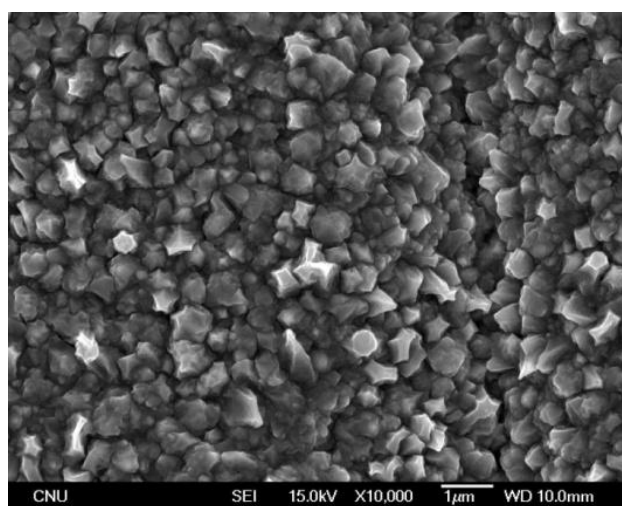
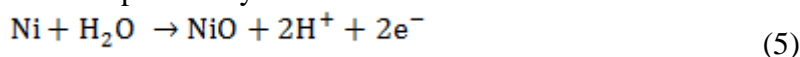


Figure 11. FE-SEM micrograph of the Raney Co/Ni 8 sample.

The origin of oxygen species in the Raney catalyst can be explained from the Pourbaix diagram [32]. It illustrates that the electrodeposition of nickel from a Watts bath has $\sim 97\%$ efficiency associated with undesirable side reactions such as oxide and hydroxide deposition could be expected. Similar to the Pourbaix illustration, in our previous work [31], we have observed NiO and $\text{Ni}(\text{OH})_2$ on the electrodeposited sample through XPS analysis. The mechanism of the formation of nickel oxide as a side reaction explained by Pourbaix is as follows:



In the Eq. 5, NiO can become hydrated NiO.H₂O or form nickelous hydroxide Ni(OH)₂. The free enthalpy of formation of NiO and Ni(OH)₂ are -51,300 cal and -108,300 cal, respectively. A negative free enthalpy of formation represents that the reaction is spontaneous but it does not imply that it is kinetically dominant. This supports the conceptual of the presence of oxide in our electrodeposited Raney samples.

The results obtained from our studies are competitive to those commonly reported for this type of material in the literature [13, 15, 17]. The best overpotential observed was for the sample 8 (-270 mV) at 100 mA cm⁻², which is within the range of 200-350 mV, where most Raney type catalyst is located. Raney nickel is a better catalyst for the HER than Raney cobalt, because in addition to high roughness factor, it is likely that nickel has a better electronic factor than cobalt. A better electronic factor is related to intermediate values of bond strength, between the active site and adsorbed hydrogen.

4. CONCLUSIONS

A porous Raney cobalt surface enhances the available area for the hydrogen evolution reaction to occur. The presence of porosity increases the efficiency of an electrodeposited material in comparison to cobalt having non-porous (i.e. smooth) surface. Raney Co showed a reasonable overpotential of -349 mV for the HER. However, when Raney Ni is added into the Raney Co coating, this improves the overpotential of the electrode substantially, exhibiting -270 mV. For all the Raney Co samples, the nickel binder competes with the catalyst, and it becomes difficult to analyze the electrochemical impedance data. Whereas, the electrochemical impedance spectroscopy fitting is found to be improved for the Raney Co/Ni mix material working at high overpotentials, where the best fitting is observed with the experimental data set. In the case of Raney Co/Ni mix, the binder does not participate for the HER (as evidenced through EIS) because the Raney Ni is a better catalyst than Raney Co and the Ni binder. FE-SEM/EDS, EIS and our previous work validate the presence of an oxide in the form of NiO and Ni(OH)₂ likely from the nickel binder.

ACKNOWLEDGEMENTS

We would like to acknowledge the Global R&D Centers Program of NRF (National Research Foundation of Korea), funded by MSIP (Ministry of Science, ICT & Future Planning) at KIGAM (Korean Institute of Geoscience and Mineral Resources) for instrument time.

References

1. W.M. Colton, The Outlook for Energy a view to 2030, in: Exxon Mobil Corporation (Ed.), 2011.
2. P. Voser, Shell Energy Scenarios to 2050 - Signals & Signposts, in: Royal Dutch Shell (Ed.), 2011.
3. P. Grundy, Shell Energy Scenarios to 2050 - Energy, in: Royal Dutch Shell (Ed.), 2011.
4. B. Dudley, BP Energy Outlook 2030, in: British Petroleum (Ed.), 2011.
5. D. Delgado, G. Hefter, M. Minakshi, Hydrogen Generation, in: G. Ferreira (Ed.) Alternative Energies, Springer, Berlin, 2013, pp. 141-161.

6. J.O.M. Bockris, A.K.N. Reddy, M. Gamboa-Aldeco, Modern Electrochemistry, Second edition ed., Kluwer Academic/Plenum Publishers, New York, 2000.
7. L.O. Garciano-II, N.H. Tran, G.S.K. Kannangara, A.S. Milev, M.A. Wilson, H. Volk, *Reac. Kinet. Mech. Cat.*, 108 (2013) 127-138.
8. W. Reeve, J. Christian, *J. Am. Chem. Soc.*, 78 (1955) 860-861.
9. J.M. Menard, Y. Trambouze, *Bull. Soc. Chim. Fr.*, (1963) 398-401.
10. R. Sassoulas, Y. Trambouze, *Bull. Soc. Chim. Fr.*, (1964) 985-988.
11. O. Savadogo, S. Levesque, E. Ndzebet, A. Martel, J. Lessard, *Int. J. Hydrogen Energ.*, 17 (1992) 101-107.
12. Y. Oda, H. Otouma, E. Endoh, Process for Preparing a Low Hydrogen Overvoltage Electrode by Decomposition Method, in: U. Patent (Ed.)U.S.A., 1983.
13. Y. Choquette, H. Menard, L. Brossard, *Int. J. Hydrogen Energ.*, 14 (1989) 637-642.
14. J.K. Dennis, T.E. Such, Nickel and Chromium Plating, 3rd ed., Woodhead Publishing, London, 1993.
15. C. Hitz, A. Lasia, *J. Electroanal. Chem.*, 500 (2001).
16. S. Rausch, H. Wendt, *J. Electrochem. Soc.*, 143 (1996) 2852-2862.
17. E. Endoh, H. Otouma, T. Morimoto, Y. Oda, *Int. J. Hydrogen Energ.*, 12 (1987) 473.
18. L.M.D. Silva, J.F.C. Boodts, L.A.D. Faria, *Electrochim. Acta*, 46 (2000) 1369.
19. J.-M. Hu, J.-Q. Zhang, C.-N. Cao, *Int. J. Hydrogen Energ.*, 29 (2004) 791-797.
20. De Faria L.A., Boodts J.F.C., T. S., *J. Appl. Electrochem.*, 26 (1996) 1195.
21. L. Valek, M. Metikos-Hukovic, Z. Grubac, *J. New Mat. Electr. Sys.*, 9 (2006) 145-153.
22. A. Lasia, Modeling of Impedance of Porous Electrodes, Modern Aspects of Electrochemistry Springer, New York, 2009, pp. 67-137.
23. A. Lasia, *J. Electroanal. Chem.*, 397 (1995) 27.
24. A. Lasia, Electrochemical Impedance Spectroscopy and its Applications, in: B. E. Conway, J. Bockris, R.E. White (Eds.) Modern Aspects of Electrochemistry, Kluwer Academic/Plenum New York, 1999, pp. 143-248.
25. A.R.J. Kucernak, V.N.N. Sundaram, *J. Mater. Chem. A*, 2 (2014) 17435-17445.
26. D. Chade, L. Berlouis, D. Infield, A. Cruden, P. T.Nielsen, T. Mathiesen, *Int. J. Hydrogen Energ.*, 30 (2013) 14380.
27. I. Herraiz-Cardona, E. Ortega, L. Vazquez-Gomez, V. Perez-Herranz, *Int. J. Hydrogen Energ.*, 36 (2011) 11578-11587.
28. B. Losiewicz, A. Budniok, E. Rowinski, E. Lagiewka, A. Lasia, *Int. J. Hydrogen Energ.*, 29 (2004) 145.
29. L. Chen, A. Lasia, *J. Electrochem. Soc.*, 140 (1993) 2464.
30. L. Chen, A. Lasia, *J. Electrochem. Soc.*, 139 (1992) 3214.
31. D. Delgado, M. Minakshi, D.-J. Kim, C. Kyeong, Electrodeposition of Raney Nickel from modified Watts bath for hydrogen generation (Unpublished work), Murdoch University, 2015.
32. M. Pourbaix, Atlas of electrochemical equilibria in aqueous solutions, Pergamon Press, California, 1966.